Materials Chemistry and Physics 248 (2020) 122909

Contents lists available at ScienceDirect

Materials Chemistry and Physics

journal homepage: www.elsevier.com/locate/matchemphys

Engineering the crystalline silicon surface by femtosecond laser processing in liquid: Hierarchical micro/nanostructure and amorphization

Jing Cao, Xingyu Shen, Zhihao Yu **, Junrong Zheng *

College of Chemistry and Molecular Engineering, Peking University, 100871, Beijing, PR China

HIGHLIGHTS

- One-step synthesis of micro/nanostructure on silicon is achieved by fs laser with the sample submerged in ethanol.
- Effects of laser pulse energy and fabrication parameters on the morphology and amorphization are investigated.
- The morphology evolution is studied by a combination of scanning electron microscope and scan probe microscope.
- Fs laser induced amorphization of crystalline silicon is demonstrated by Raman spectroscopy.

GRAPHICAL ABSTRACT

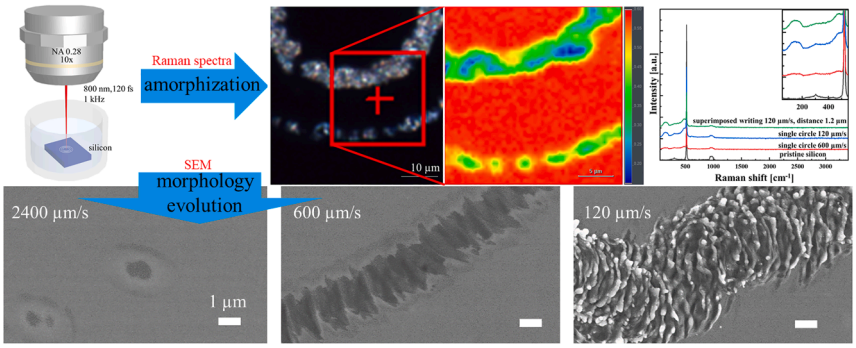

ARTICLE INFO

Keywords:
Black silicon
Topographical surface alterations
Femtosecond phenomena
Laser ablation in liquid

ABSTRACT

Hierarchical micro/nanostructure surface structures with different spatial characteristics are achieved after irradiation of crystalline silicon via femtosecond (fs) laser pulses (800 nm, 120 fs, 1 kHz) with the sample submerged in ethanol. According to laser pulse energy and fabrication parameters (such as scanning speed and superimposed writing), a characteristic morphology evolution of ovoid-like smooth modified area, ripple-like, wave-like, and coral-like micro/nanostructures is demonstrated, and the underline principle is discussed. The amorphization of fs laser-modified area is verified and investigated by Raman spectroscope. These modified structures have potential applications in sensors, silicon photovoltaic cells, and sterilization.

1. Introduction

Fabrication of hierarchical micro/nanostructures on crystalline silicon surface is an efficient approach to achieve enhanced properties (e.g. superoleophobicity [1] and anti-reflectance [2]), which could have enormous potential applications in surface-enhanced Raman scattering substrate [3], antifouling coating [4], and advanced optoelectronics devices [5]. Various techniques have been implemented to achieve hierarchical micro/nanostructures on silicon. Typically, photolithography is adopted but this process is time-consuming, multistep, and complex photo mask designs are needed [6]. Metal assisted chemical etching is an alternative to obtain uniformity and large-scale micro/nanostructures, but this method is tedious and hazardous etchants (e.g. HF) may be employed, and the caused metal pollution is not compatible with the

* Corresponding author.
** Corresponding author.
E-mail addresses: zhihaoyu@pku.edu.cn (Z. Yu), junrong@pku.edu.cn (J. Zheng).

https://doi.org/10.1016/j.matchemphys.2020.122909
Received 29 October 2019; Received in revised form 1 March 2020; Accepted 6 March 2020
Available online 7 March 2020

following complementary metal oxide semiconductor (CMOS) process [7]. In particular, the versatile laser texturing strategy has distinguished itself by its flexibility, rapid mask-less single-step process, large-scale fabrication, eco-friendly operation, and multiparameter adjustment [1,4,7].

Compared with continuous wave lasers or long pulsed lasers (e.g. ns lasers), ultrafast lasers (e.g. fs lasers) can dramatically reduce the heat destruction due to the shorter pulse duration (i.e. much shorter than the electron-phonon energy relaxation time) [5,8]. The light intensity of a focused fs laser can reach as high as several TW/cm^2, thus inducing multi-photon ionization or/and tunnelling ionization. As the absorption is non-linear, it occurs only in the focal volume [9]. The texturing exhibits unique properties such as high fabrication accuracy and processing quality [10–13]. It is reported that the morphology of ripples obtained by ultrashort laser pulses is more complex, compared with the ones obtained by long laser pulses [14]. It is demonstrated that the optoelectronic devices manufactured by fs laser hyper doping show photo response at longer wavelengths and in thinner layers than those prepared using ns laser; by controlling the surface morphology, the fs laser induced hyper doping can be adjusted [15]. Moreover, remarkable absorptance of modified silicon lattice can be enhanced by surface texturing [16]. Investigating the laser induced modifications (e.g. morphology), specially the ultrafast ones, is challenging and meaningful for a better understanding of the mechanism of ultrafast laser-matter interaction and providing distinct hierarchical micro/nanostructure surface structures for novel applications. Considering fs laser induced micro/nanostructure morphology is very sensitive to fabrication parameters [9,11], it is essential to have a parameter guide before performing the fs laser irradiation to achieve the desired micro/nanostructures.

Various micro/nanostructure formations can be achieved by fs laser irradiation of silicon under different gas environments (e.g. Cl_2, H_2S, and SF_6) [17] or pressure [18]. However, the application of gas environment causes extra steps and operation complexity, and some gases are hazardous. It is urgent and significant to obtain micro/-nanostructures on silicon with a simpler and safer strategy. With respect to fs laser texturing in air, the fabrication in liquids has received extensive attention owing to its advantages such as lower debris left, unique formations of micro/nanostructures, enhanced material removal rates, and the versatility of liquid options [19,20]. Because of the liquid's higher specific heat capacity and thermal conductivity, the thermal load can be dramatically reduced. It is demonstrated that the presence of water and the associated increased cooling rate of the molten layer, allows the formation of nanoscale ripple-like structure [11]. Additionally, liquids can affect the surface chemical modifications (e.g. lesser extent of the processed surface oxidation) [19]. Thus, it is important and practically significant to explore the mechanisms of ultrafast laser-matter interaction during the ultrafast laser induced micro/-nanostructure in liquids and to provide the correlation between fs laser induced hierarchical micro/nanostructures and laser fabrication parameters (e.g. scanning speed and superimposed writing), thus guiding further engineering the crystalline silicon surface.

The fs laser irradiation can induce the amorphization of silicon, which may have an influence on its electrical or optical properties, thus affecting its applications [21], or can be used as mask-less lithography [6]. In particular, the fs laser irradiated crystalline silicon can undergo complex transformations during laser ablation and structure formations (a non-equilibrium phase transition process) [22,23]. Therefore, it is necessary to provide the amorphization information (e.g. the inhomogeneity and distribution) of fs laser irradiated silicon in liquids as well.

Herein, a thorough investigation is conducted on how to accurately control the fs laser induced hierarchical micro/nanostructures on crystalline silicon with sample submerged in ethanol. For comparison, the fabrication by fs laser in air is also performed. With adjustable combinations of irradiation parameters (e.g. laser pulse energy and scanning speed) and fabrication geometry (the distance between each irradiated circle or superimposed writing), various morphologies are achieved on silicon. Finally, the inhomogeneity and distribution of fs laser induced amorphization of crystalline silicon are demonstrated by Raman spectroscopy.

2. Material and methods

Commercially available two-side polished P-type (boron doped) <100> oriented silicon (with thickness of 725 ± 20 μm) wafers are used as substrates. Prior to laser fabrication, these wafers are cleaned by sonication in ethanol for five minutes for three times. Although water is a commonly used liquid medium in fs laser fabrication [11,19], liquid with a lower boiling point is more effective in reducing the formation of debris and the drilled hole taper angle in silicon [20]. Herein ethanol, with a lower boiling point than that of water and a very low extent of toxicity, is employed as the liquid medium. The experiments are performed in ambient air and in ethanol with a liquid depth of approximately 3.7 mm, as shown in Fig. 1. The cleaned silicon is immersed in an ethanol bath. A linearly-polarized femtosecond pulse laser (UpTek Solutions, model: Phidia-c) with central wavelength of 800 nm, a pulse length of 120 fs, and repetition rate of 1 kHz is used as the irradiation source. The laser pulse energy is adjusted by a combination of λ/2 plate and Glan-Taylor calcite polarizer. The pulse energy is measured just before the beam passing through the objective lens. The laser beam is focused by a 10X objective lens (NA = 0.28 and WD = 34.0 mm) onto the surface of the sample. Instead of the straight lines writing, circular trajectories are investigated here for the further complex pattern design. The interval of adjacent writing circle and writing speed (i.e. 120–2400 μm/s) are controlled by a galvanometric scanner. The sample is totally dried before the following measurements.

The morphology and the hierarchical micro/nanostructure of fs laser irradiated silicon are investigated by a field emission scanning electron microscope (SEM, Hitachi S-4800). The topography of the laser-modified surface is investigated by an atomic force microscopy (AFM),

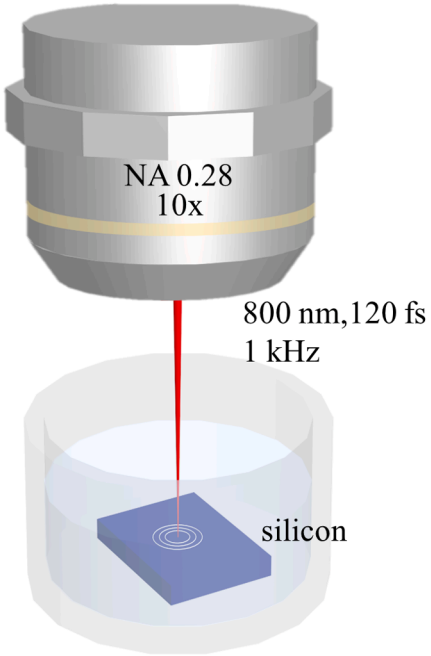

Fig. 1. Experimental setup of femtosecond laser processing in a liquid environment. The incident beam is focused by an objective lens (10X, NA = 0.28, and WD = 34.0 mm) onto the sample surface immersed in ethanol from the top. Laser irradiated concentric circles pattern is performed with various distances and scanning speeds.

recorded by a scan probe microscope (SPA400) in the contact mode with a scan speed of 1.00 Hz. The amorphization of fs laser irradiated silicon is recorded on a micro Raman imaging spectrometer (DXRxi) at room temperature with excitation at 532 nm, a 50X objective, and a 50 μm confocal pinhole. The image pixel size of Raman spectral mapping is 0.5 μm. It is worth pointing out that the Raman excitation laser exposure may cause solid phase transformation of silicon, taking several hours when it is thermally activated, but typical Raman measurements of laser exposure are at the scale of second [24]. Considering the instability of amorphous phase, to avoid any damage during the Raman measurement (e.g. laser induced melting), a low laser power 1.5 mW is used here [25].

3. Results

3.1. fs laser induced micro/nanostructure on silicon

Fig. 2 presents the scanning electron microscope (SEM) images of fs laser-modified silicon surface in ethanol according to various combinations of laser pulse energy and scanning speed for single circle writing. Taking the scanning speed 2400 μm/s for example (the first column of Fig. 2), for the case of the lowest laser pulse energy (i.e. 56 nJ/pulse), ovoid-like smooth modification is obtained with the inner core diameter around 740 nm and the outer diameter 2300 nm. When the laser pulse energy is raised to 80 nJ/pulse (the middle image of the first column of Fig. 2), a similar ovoid-like smooth structure is obtained but with the inner diameter increases to around 2200 nm and the outer goes to approximately 3200 nm. The ratio between the two diameters increases dramatically from 32% to 69%. If we continue to increase the pulse energy to 240 nJ/pulse (the bottom image of the first column of Fig. 2), a well-defined ripple-like structure occurs on each dot, with a width of 893 ± 113 nm and a period of 975 ± 98 nm. The period of the ripple-like structure is close to the used fs laser wavelength (i.e. central wavelength of 800 nm), which can be explained by the interference between the incident laser and the surface electromagnetic wave, which also can explain the nanostructures obtained by long pulsed lasers or continue wave lasers [26]. This indicates that even at a relatively low repetition rate of 1 kHz, there is still an energy threshold over which the thermal effect can overwhelm the predesigned hierarchical micro/-nanostructure. It is worth pointing out that at this high scanning speed (2400 μm/s), there is no overlap effect between each fabrication dot, and only separated dots are observed along the scanning direction.

Scanning speed is an important parameter in laser fabrication, which determines the number of laser-shots at a spot, and thus affects the fabrication result. When the scanning speed is decreased to 1500 μm/s (the second column of Fig. 2), at 56 nJ/pulse, there is no special structural feature from that at the higher speed one (i.e. 2400 μm/s) but the ovoid-like smooth modified pattern. However, at 80 nJ/pulse (the middle image of the second column of Fig. 2), using lower scanning speed can dramatically affect the structure: a ripple-like structure is recorded with a width of 978 ± 223 nm, a length of 4181 ± 394 nm, and a period of 1034 ± 154 nm. Similar structures are obtained at 240 nJ/pulse with a width of 860 ± 112 nm, a length of 6981 ± 290 nm, and a period of 876 ± 66 nm (the bottom image of the second column of Fig. 2). When we continue to decrease the scanning speed to 600 μm/s (the third column of Fig. 2), a denser ripple-like structure appears. With the increase of laser pulse energy from 56 to 80 nJ/pulse, the widths of ripple-like structure are 539 ± 50 nm and 563 ± 117 nm, respectively, with respective lengths of 2573 ± 173 nm and 4318 ± 260 nm. However, in the event of 240 nJ/pulse, a bit disordered wave-like structure is observed, accompanied with a ripple-like structure with a width of 528 ± 64 nm and a period of 510 ± 81 nm. Interestingly, when the scanning speed is reduced to 120 μm/s (the last column of Fig. 2), a much denser micro/nanostructure is formed with some elongated extensions at the edge of the structure at 56 nJ/pulse. At a higher pulse energy of 80 nJ/pulse, some coral-like structures occur with more protrusions. This phenomenon becomes very clear at an even higher pulse energy (i.e. 240 nJ/pulse, the bottom image of the fourth column of Fig. 2), a disordered coral-like structure with olive-like protrusions. Meanwhile, the micro/nanostructures could maintain the structure even when bending the scanning direction, which is promising in further design of complex trajectories.

Superimposed writing (i.e. a wring pattern in which there is an interaction between neighboring lines) can also affect the laser fabrication result. Fig. 3 displays the superimposed writing (four circles with a distance of 1.2 μm) at different combinations of pulse energy and scanning speed. As we can see from the top and middle of the first column or the top of second column of Fig. 3, an ovoid-like smooth structure is obtained. However, at a higher laser fluence (bottom of the first column or middle and bottom of second column or top of the third column of Fig. 3), we observe some disordered wave-like structures. At

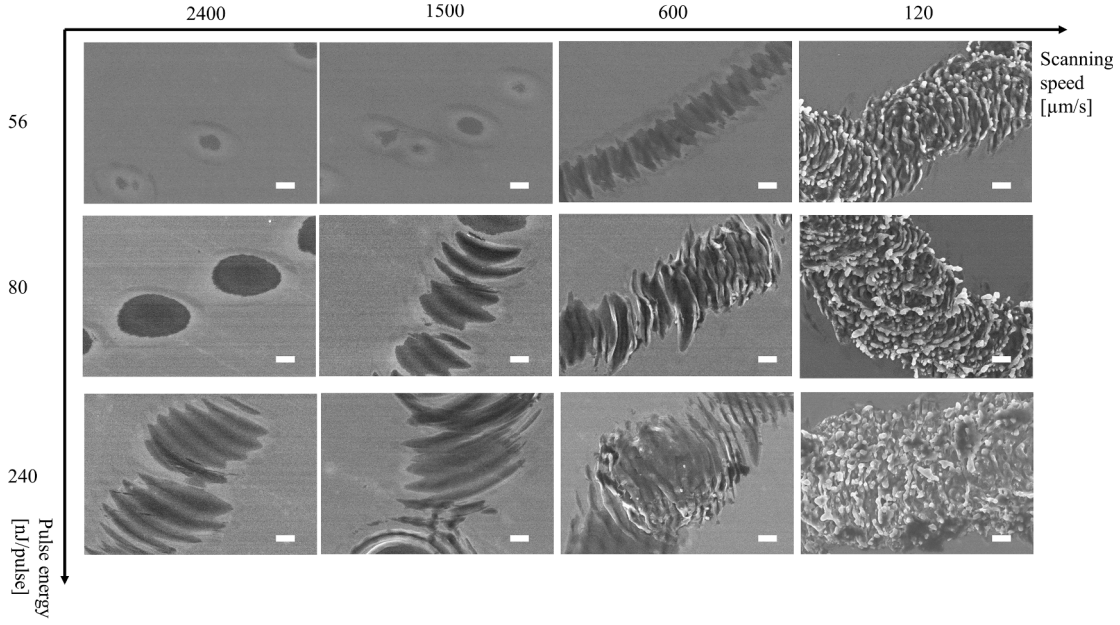

Fig. 2. SEM images of fs laser induced micro/nanostructure on silicon of single circle at various combinations of laser pulse energy and scanning speed in ethanol. All scar bars are 1 μm.

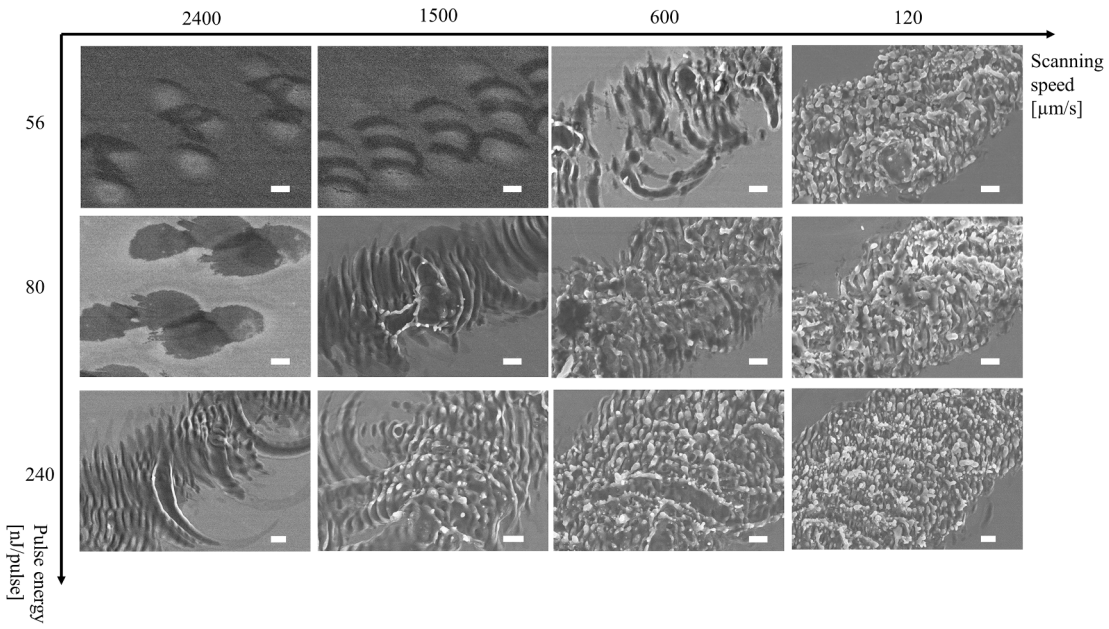

Fig. 3. SEM images of fs laser induced micro/nanostructure on silicon of with superimposed writing (four circles with a distance of 1.2 μm) at various combinations of laser pulse energy and scanning speed in ethanol. All scar bars are 1 μm.

56 nJ/pulse and 600 μm/s, the width of the pattern is 529 ± 38 nm with a period of 520 ± 28 nm. In the case of 80 nJ/pulse and 1500 μm/s, the width is 524 ± 47 nm with a period of 530 ± 94 nm. At 240 nJ/pulse and 2400 μm/s, the width is 530 ± 41 nm with a period of 552 ± 48 nm. All of these widths and periods are smaller than those without superimposition (Fig. 2). When we continue increasing the laser fluence, coral-like structures appear with a larger amount of protrusions (illustrated in bottom of third column or last column of Fig. 3).

In comparison, surface topography of silicon, ablated in air at various combinations of laser pulse energy and fabrication parameter, is investigated. As shown in Fig. 4a, an ovoid-like smooth modification is observed at a combination of low pulse energy and high scanning speed (i.e. 56 nJ/pulse and 2400 μm/s), which is similar to the ones fabricated in ethanol. However, instead of a coral-like micro/nanostructure observed in ethanol at a lower scanning speed, a well-defined ripple-like structure (with a width of 374 ± 80 nm and a period of 694 ± 112 nm) with some spatter is obtained in air, as presented in Fig. 4b. For the superimposed writing, illustrated in Fig. 4c, the ripple-like structure is separated by holes and more debris appears. As shown in Fig. 4d, at a higher pulse energy and a faster scanning speed (80 nJ/pulse, 2400 μm/s), ripple-like structures (with a period of 773 ± 58 nm) appear on smooth ovoid-like dots. A larger scale ripple-like structure with an increased width of 455 ± 125 nm and a period of 798 ± 84 nm is obtained at this laser pulse energy with a modest scanning speed for superimposed writing (Fig. 4e). It is worth noting that at a low scanning speed and superimposed writing mode (Fig. 4f and 120 μm/s), grooves and olive holes (with the major axis of 583 ± 79 nm) are detected with an increase of quantity and size of the debris. These results reveal that liquid-assisted fs laser texturing on silicon can efficiently flush away debris or spatters on the periphery of fs laser-modified region, compared with the ones fabricated in air, which is significant in the further semiconductor applications [20].

To investigate the height information of the fs laser induced micro/nanostructure, AFM measurements are conducted. As shown in the 3D AFM image (Fig. 5a), with the single circle writing (the top SEM image of the third column of Fig. 2), the peak-to-valley height is around 25 nm. In contrast, with the superimposed wring (Fig. 5b), a well-defined ripple-like structure, with a deeper structure with the peak-to-valley height

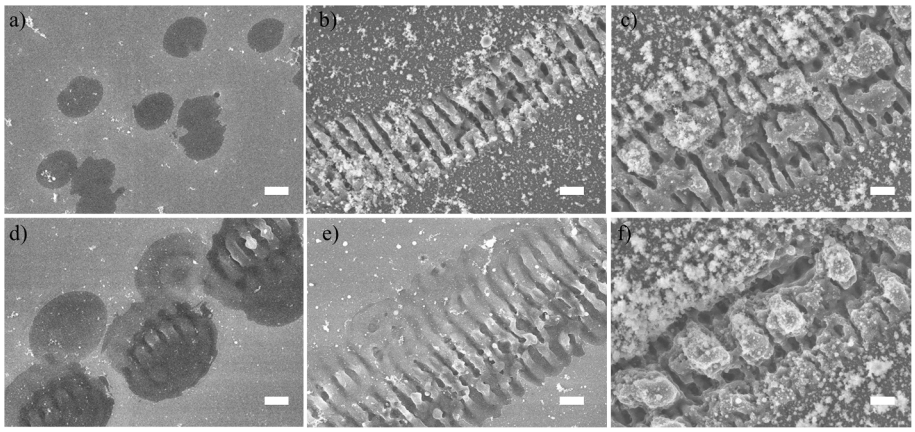

Fig. 4. SEM images of fs laser induced micro/nanostructure on silicon in air at a) 56 nJ/pulse, 2400 μm/s, four circles with a distance of 1.2 μm, b) 56 nJ/pulse, 120 μm/s, single circle, c) 56 nJ/pulse, 120 μm/s, four circles with a distance of 1.2 μm, d) 80 nJ/pulse, 2400 μm/s, four circles with a distance of 1.2 μm, e) 80 nJ/pulse, 1500 μm/s, four circles with a distance of 1.2 μm, and f) 80 nJ/pulse, 120 μm/s, four circles with a distance of 1.2 μm. All scar bars are 1 μm.

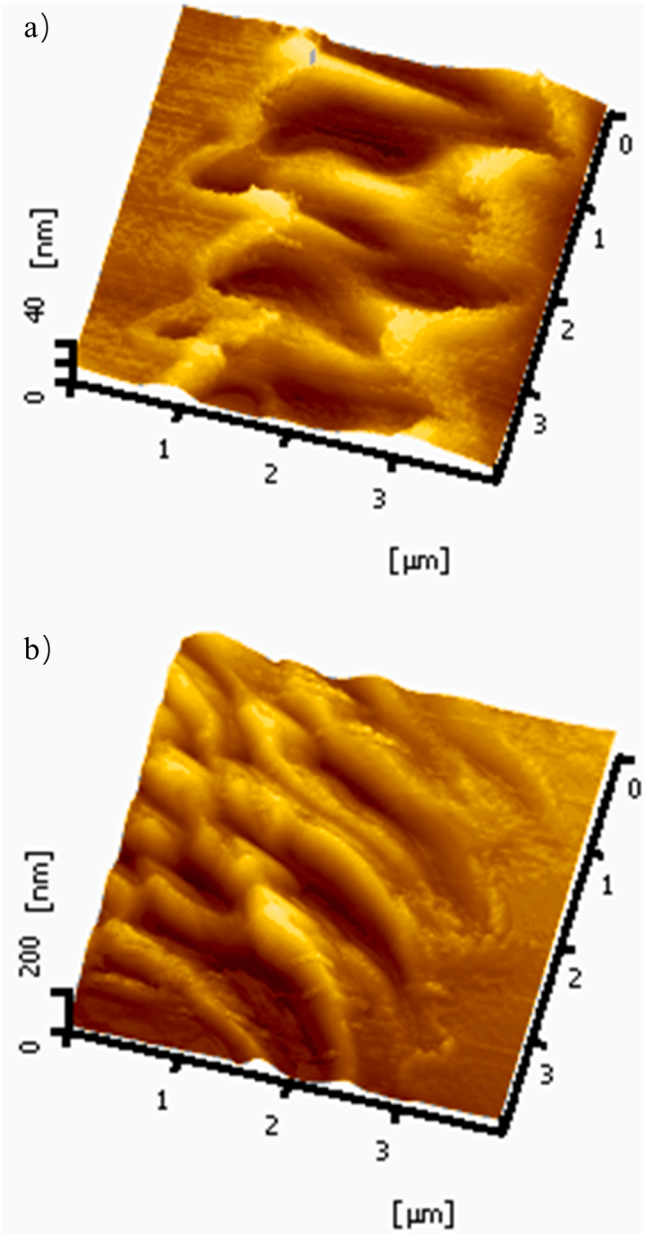

Fig. 5. Topographies of the fs laser induced micro/nanostructure on silicon investigated with AFM: a) single circle and b) superimposed writing (four circles with a distance of 1.2 μm) in ethanol at 56 nJ/pulse and scanning speed 600 μm/s.

approximately 100 nm, appears. It is worth pointing out that for the low fs laser fluence modified structure (Fig. 5a), some structures are below the pristine silicon surface, indicating the net ablation dominant. However for a high laser fluence (Fig. 5b), the formed structure is above the original surface, indicating the mechanism by deposition and growth [17].

3.2. fs laser induced amorphization on silicon

Micro Raman spectroscopy measurements are performed on the modified silicon surface to investigate the amorphization that can occur. Two vibrational bands are related to the contributions of the microcrystalline and amorphous phases: the dominant sharp peak centered around 520 cm^{-1} is attributed to the transverse optical (TO) mode of Si–Si vibrations in the crystalline phase; the broad peak located around 480 cm^{-1} is due to the TO mode of the stretching vibration mode of Si–Si bonds of the amorphous silicon network [21].

Fig. 6a displays the Raman spectra of fs laser-modified area fabricated at various parameters (i.e. scanning speed and single circle or superimposed writing modes) and the pristine silicon. Compared with the pristine silicon, under single circle fs laser irradiation at a fast scanning speed (red curve, 600 μm/s), a broad and continuous peak, located at approximately 480 cm^{-1} occurs (clearly shown in magnification of the inset of Fig. 6a), indicating the fs laser induced amorphization. This phenomenon becomes more apparent at a lower scanning speed (blue curve, 120 μm/s). With the superimposed writing, the amorphous state becomes even more salient (green curve, 120 μm/s, four circles with a distance of 1.2 μm). Besides the peak at around 480 cm^{-1}, a broad peak centered around 150 cm^{-1} also appears accompanying the fs laser fabrication (clearly demonstrated in magnification of the inset of Fig. 6a). A similar peak is also observed in glass and other amorphous materials [27]. In general, it is attributed to the Boson mode associated with the excess density of quasi-local acoustic vibrations in the corresponding frequency range, which arises from the lack of long-range order in these materials and the violation of translational symmetry. Amorphous silicon exhibits a broad band approximately 480 cm^{-1}, with a hump around 350 cm^{-1} and is also accompanied by a small peak around 150 cm^{-1}. Its peak position appears between any value between 475 and 490 cm^{-1}, depending on the preparation method [28]. The peaks at around 950 cm^{-1} diminish as the amorphization increases. These peaks belong to the SiOH vibrations of the oxide layer of Si wafer. Their disappearance indicates the amorphization requires the removal

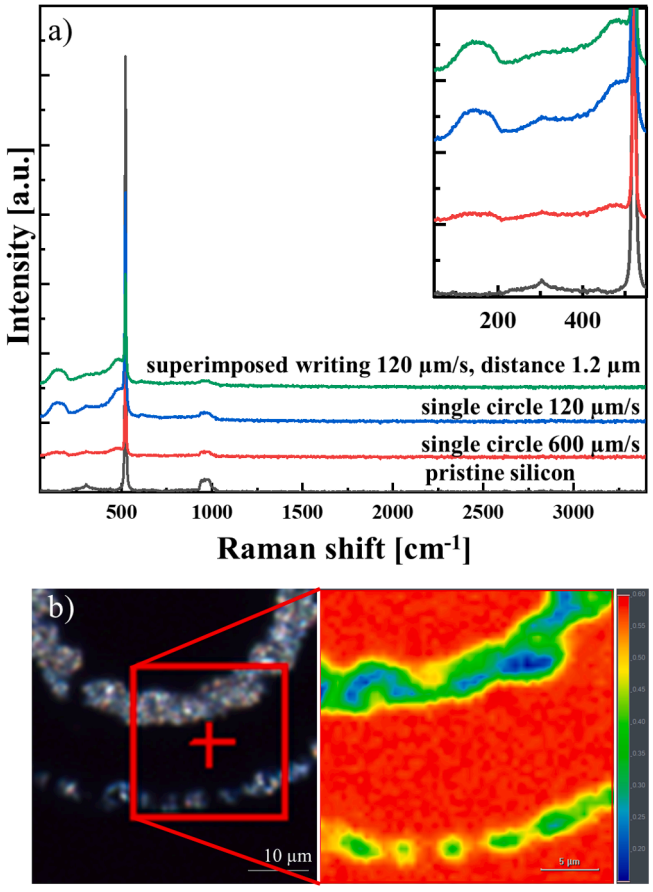

Fig. 6. a) Raman spectra of the pristine silicon and fs laser irradiated zones in ethanol with varying fabrication parameters, indicated around each curve (the inset is the magnification), b) Raman spectral mapping of the irradiated zone in ethanol (fs laser pulse energy 56 nJ/pulse, single circle writing pattern, the inner circle is at 120 μm/s, the out circle is at 600 μm/s scanning speed).

of the surface oxide layer.

The Raman spectral mapping of the laser irradiated circles pattern is illustrated in Fig. 6b. At a fixed pulse energy (i.e. 56 nJ/pulse), with the increase of scanning speed (the inner circle is at 120 μm/s and the out circle is at 600 μm/s), the amorphization zones become smaller. We observe an amorphization gradient from the center of the modified area to the margin (i.e. from blue to green then to yellow until the red silicon background). Interestingly, a clear boundary (illustrated by yellow in Fig. 6b) is observed around the silicon background and the laser-modified region.

4. Discussion

4.1. Summary of the fs laser induced hierarchical micro/nanostructure

Fig. 7 displays the quantitative analysis of the relationship between the fs laser pulse energy and the width, length, and period of fs laser induced ripple or wave-like hierarchical micro/nanostructure at various scanning speeds and writing modes (i.e. sing circle or superimposed mode) on silicon in ethanol. As illustrated in Fig. 7a, at a low laser pulse energy (e.g. 56 nJ/pulse) and 600 μm/s, there is no big difference in the width between the single circle or superimposed mode (i.e. four circles with a distance of 1.2 μm): 539 ± 50 nm and 529 ± 38 nm, respectively. However, at a higher pulse energy (80 nJ/pulse) and 1500 μm/s, the width decreases dramatically from single circle to superimposed writing (i.e. from 978 ± 223 nm to 524 ± 47 nm). Similar results are achieved for the case of 240 nJ/pulse, 2400 μm/s (i.e. 893 ± 113 nm and 530 ± 41 nm, respectively). In addition, the width of the ripple-like micro/nanostructure increases with the scanning speed for single circle writing. For example, at 80 nJ/pulse, with the increase of scanning speed from 600 to 1500 μm/s, the width varies from 563 ± 117 nm to 978 ± 223 nm. For the case of 240 nJ/pulse, from 600 to 1500–2400 μm/s, it increases steeply from 528 ± 64 to 860 ± 112 nm then slightly to 893 ± 113 nm. For the lengths of the hierarchical micro/nanostructure (displayed in Fig. 7b), they are bigger at superimposed mode than the single circle writing one. As for the period (illustrated in Fig. 7c), for 80 nJ/pulse, 1500 μm/s, writing, we observe an abrupt decrease of period from 1034 ± 154 nm to 530 ± 94 nm from single circle writing to superimposed mode. Similar phenomena are observed for 240 nJ/pulse, 2400 μm/s, in which the periods are 975 ± 98 nm and 552 ± 48 nm for single circle writing and superimposed mode, respectively. It indicates that the fs laser induced micro/nanostructure morphology is strongly fabrication parameter dependent, which is significant to provide a parameter guide before the fs laser fabrication.

4.2. Formation of hierarchical micro/nanostructure on silicon

Laser power plays a vital part in the rate of energy deposition per unit area, thus affecting the morphology of micro/nanostructures [9]. Shen et al. [11] report that with the increase of laser fluence (800 nm, 100 fs, 1 kHz), the interaction between laser and silicon/water system can be classified as following: below the silicon ablation threshold, ultrafast melting and re-solidification with period of ripples at nanoscale (120 nm); ultrafast melting and ablation with period of ripples equal to the laser wavelength; ultrafast melting, ablation, and bubble cavitation with the formation of microscale structures and sub-micro holes. Tull et al. [17] demonstrate the surface morphology evolution of silicon according to pulse numbers in SF_6 (800 nm, 100 fs, 1 kHz): the first pulse causes small defects randomly distributed over the silicon surface, exhibiting circular shape due to the burst bubble that is frozen in place upon melt re-solidification; after the second pulse, ripple-like structures occur; after five laser pulses, the ripple disappears but with small beads; after ten pulses, the early formation stage is over and the final morphology is established; from ten to several hundred pulses, conical-like structures appear and finally with sphere perched on the cone, which is similar to the ones obtained by ns laser irradiation. It is interesting to point out

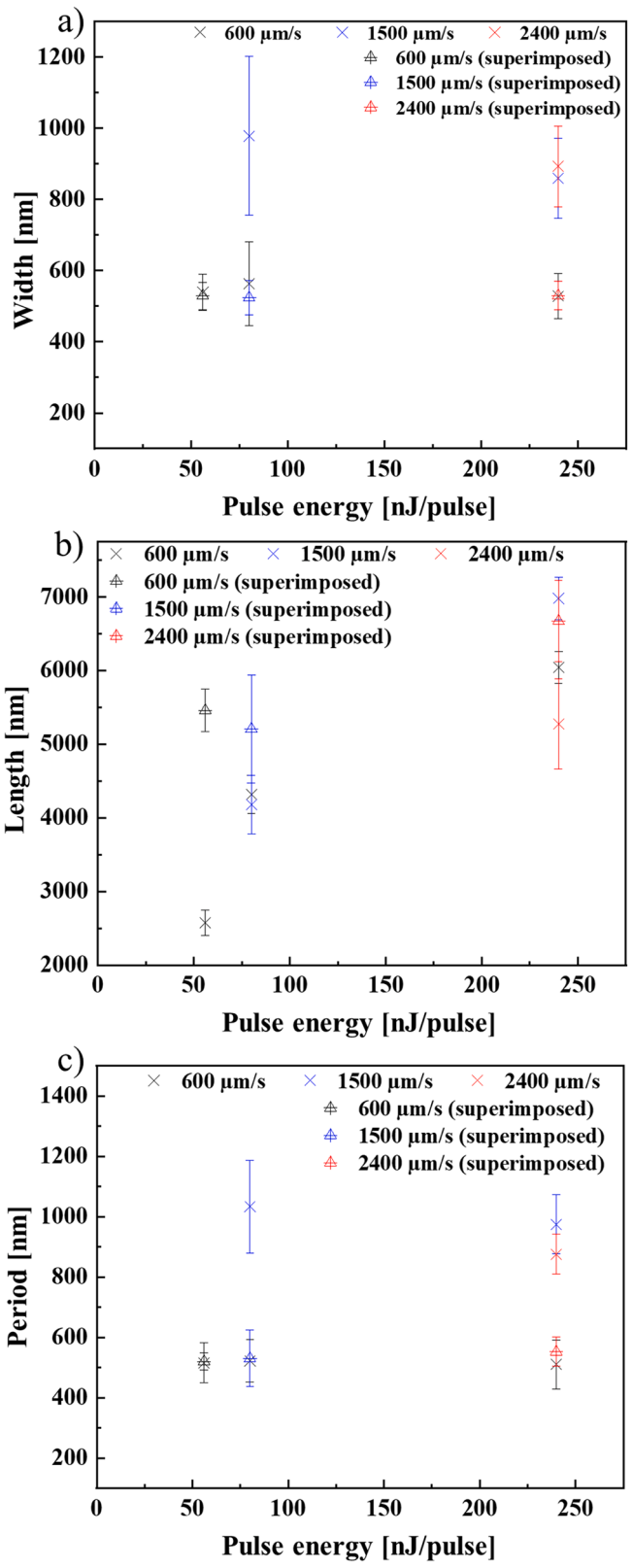

Fig. 7. Quantitative analysis of the relationship between the fs laser pulse energy and the a) width, b) length, and c) period of fs laser induced hierarchical micro/nanostructure on silicon in ethanol.

that the cone's tip is at or below the original surface, indicating that these cones are formed by a net ablation instead of by deposition and growth. In addition, liquid medium causes high aspect ratio submicron spikes formation; chemically active gases (e.g. SF_6) have an influence on silicon micro cones' shape; gas pressure generally plays a part in the micro cones' size [5].

Typically, there are two distinct kinds of laser induced periodic surface structures (LIPSS, termed as ripples) with the energy below or close to the material ablation threshold: low-spatial-frequency LIPSS and high-spatial-frequency LIPSS [14]. With the increase of laser fluence, the LIPSS progressively evolves in microstructures (e.g. conical-like structure) [17]. The period of low-spatial-frequency LIPSS is close to the laser wavelength and can be elucidated by the interference of the incident laser light with the surface electromagnetic wave and this model can successfully explain the results obtained by continue wave laser or ns laser [26]. The period of the high-spatial-frequency LIPSS is much smaller than the laser wavelength and the mechanism is still quite controversial, which may be explained by several models such as self-organization and second-harmonic generation [29]. It is worth pointing out that due to the complexity of fs laser-matter interaction, some complex structures (e.g. periodic nanoscale phase separation [9]) can be obtained and the mechanisms are yet to clarify.

Based on the above discussion, the obtained ovoid-like smooth modification on silicon displayed in Fig. 2 (top and middle of first column) is due to the melt re-solidification. The recorded ripple-like structure with period around laser wavelength can be explained by the classic interference between the incident laser light and the laser induced surface plasmons. For the elongated structure (shown in Fig. 2 last column), it can be explained by thermocapillary flow. The temperature gradient between the melt pool and the surrounding creates a surface tension gradient: the surface tension of the innermost of hot melt pool is lower than that of the outermost of the melt-pool [30].

Lower laser fluence removes minimal material from the surface. In contrast, at higher laser fluence, plasma density becomes higher and ablation is enhanced and thus the material can be ablated more efficiently. The interference between laser and light scattered by minor surface defects can also result in inhomogeneous energy deposition at higher energy deposition case (e.g. the case in Fig. 3 last column). Especially, for the superimposed writing, the existence of the previously discussed structures (i.e. the ripple-like structure or protrusions) are helpful for the following laser being coupled deeper onto material due to the geography [17]. Due to the melting of silicon, the nucleation of the liquid silicon appeared at interface, forming separated olive-like protrusions on the top (bottom image of the last column of Fig. 3). The bubble formation during fs laser fabrication may also contribute to the disorder of structures at high laser fluences. A lower writing speed deposits more energy at each spatial position. On the contrary, a higher writing speed leads to minimal ablation to create micro/nanostructures. A lower scanning speed (i.e. 120 μm/s in our experiment) provides a higher laser fluence at each spot, leading to higher laser ablation. Meanwhile, at a low scanning speed the removal of silicon chunks leads to a higher inter-microstructure distance.

Remarkably, the debris around the micro/nanostructure is significantly reduced with the assistance of ethanol than that of air. This is probably because the plasma is confined in the liquid, leading to higher acoustic and shock waves. Meanwhile, the formed bubbles, accompanied with shock waves, also contribute to the reduction of laser ablation induced debris [20].

These results reveal that just by controlling the combination of fs laser pulse energy, scanning speed, and writing pattern, alternative micro/nanostructures (i.e. an evolution from ovoid-like smooth modification to ripple-like, wave-like, and coral-like structures with the increase of laser fluence) with lower debris can be obtained on silicon in ethanol. Especially, high scanning speed laser texturing of crystalline silicon is of commercially interest.

4.3. Amorphization of silicon

By carefully controlling the fs laser fluence under the ablation threshold, crystalline silicon can have a transition to the amorphous state [6,23]. The formed amorphous phase can be explained by the rapid cooling of liquid silicon. In details, after the rapid heating due to fs laser irradiation, a molten region is created and the subsequent rapid cooling of liquid silicon transforms it to amorphous state [31]. Izawa et al. [32] report that the thickness of the amorphous silicon induced by ultraviolet fs laser irradiation is closely correlated with the depth of melting. Bai et al. [21] demonstrate that the geography (i.e. fs laser induced nanoripples) can reduce the silicon surface reflectance during fs laser ablation, leading to a high degree of amorphization of silicon. Costache et al. [23] demonstrate the phase transformations in the fs laser irradiated spot (800 nm, under ultrahigh vacuum) of crystalline silicon (100) from Si–I to the polymorphs Si-III, Si-IV, Si-XII, amorphous silicon, and a hexagonal Si-wurtzite phase. In the thermal affected region, the amorphous silicon is abundant. Ionin et al. [22] show that fs laser (1030 nm, 300 fs) can induce micron-deep positions of amorphous nano inclusions and high-pressure Si-III and Si-XII nanocrystalline polymorphs.

The amorphization gradient recorded from the center of the modified region to the edge (Fig. 6b) is because of the Gaussian-like beam intensity distribution, where the fs laser fluence is the highest at the center zone. Meanwhile, the obtained ripple-like micro/nanostructure may also be beneficial to the amorphization of silicon. It is worthwhile mentioning that during fs laser ablation, because of the high pressure, the liquid silicon phase may be pushed out the molten material and forced to above the surface [31]. When the liquid solidifies to the amorphous state, protrusions appear, which may explain the observation of large amount of protrusions in the last column at the bottom of Fig. 3. That very few SiH or CH stretches, observed in Raman spectroscopy measurements, indicate that during the formation of the melt state, very few Si or H or CH radicals are generated by the fs laser irradiation.

Generally, the peaks around 920 cm^{-1} and 1079 cm^{-1} can be due to the generation of Si-$(OH)_x$ and the bonds around 820 cm^{-1} can be related to Si–O–Si [33]; the peak at 896 cm^{-1} has been assigned to a resonance Raman scattering of oxygen dangling bonds (i.e. non-bridging oxygen hole centers) [34], which are not obviously identified here after fs laser irradiation. Three stretching modes at 2000 cm^{-1}, 2090 cm^{-1}, and 2120 cm^{-1} can be assigned to different ordered hydrides (i.e. SiH, SiH_2, and SiH_3, respectively) [35]. As shown in Fig. 6a, no salient peaks at around 2000 cm^{-1} and 2800 cm^{-1} are observed in the amorphous regions, indicating that very few Si–H and Si-OC_2H_5 bonds have formed during the fs laser fabrication.

Sun et al. [36] show that laser induced defects in silicon is laser fluence dependent: below laser melting, no defects are detected; between laser melting and ablation, oxygen incorporation and point defects are dominated; above laser ablation, strain and dislocations are mainly generated; under laser annealing, structural defects can be remarkably eliminated. Wu et al. [16] report that the incorporation of a high density of impurities and structural defects (i.e. introducing infrared absorbing states near the band edge) into the silicon lattice may lead to a higher infrared absorptance of the modified crystalline silicon. When the dopant is the heavy chalcogen (e.g. selenium and sulfur), the doped Si shows unique optical properties [15]. Kudryashov et al. [4] demonstrate that sulfur doped (~3 atom %) Si nanosheets, under a 5 mm carbon disulfide liquid layer, exhibit a strong infrared absorbance. Investigating further the defects/damages properties of this fs laser-modified surface structures will throw light on to the potential optoelectronic applications.

5. Conclusions

In conclusion, we conduct a comprehensive investigation of surface engineering of crystalline silicon by a flexible and controllable

technique, fs laser irradiation (800 nm, 120 fs, 1 kHz). The effects of laser pulse energy, scanning speed, writing distance, and fabrication environment (in air or in liquid) on the laser-modified surface topography are investigated. It demonstrates that fs laser can induce various types of micro/nanostructures such as an ovoid-like smooth, coral-like, ripple-like, wave-like structures or grooves, or holes, just by adjusting the laser fabrication parameters. Moreover, the amorphization of silicon can also be controlled. This paper can serve as a guide to the fs laser texturing of silicon with alternative hierarchical micro/nanostructure regions according to fabrication parameters. This topic may open up the designs of surface engineering silicon into applications in photonics and electrics.

Disclosures

The authors declare no conflicts of interest.

Declaration of competing interest

The authors declare that they have no known competing financial interests or personal relationships that could have appeared to influence the work reported in this paper.

CRediT authorship contribution statement

Jing Cao: Conceptualization, Writing - original draft, Methodology. **Xingyu Shen:** Methodology, Validation. **Zhihao Yu:** Methodology, Investigation. **Junrong Zheng:** Supervision, Writing - review & editing.

Acknowledgments

We acknowledge financial support from the National Natural Science Foundation of China (NSFC-21627805, 21673004, 21804004, and 21821004) and MOST (2017YFA0204702) China.

References

[1] J. Yong, F. Chen, Q. Yang, Z. Jiang, X. Hou, A review of femtosecond-laser-induced underwater superoleophobic surfaces, Adv. Mater. Interfaces 5 (2018) 1701370, https://doi.org/10.1002/admi.201701370.
[2] V. Parmar, Y.C. Shin, Wideband anti-reflective silicon surface structures fabricated by femtosecond laser texturing, Appl. Surf. Sci. 459 (2018) 86–91, https://doi.org/10.1016/j.apsusc.2018.07.189.
[3] E.D. Diebold, N.H. Mack, S.K. Doorn, E. Mazur, Femtosecond laser-nanostructured substrates for surface-enhanced Raman scattering, Langmuir 25 (2009) 1790–1794, https://doi.org/10.1021/la803357q.
[4] S.I. Kudryashov, L.V. Nguyen, D.A. Kirilenko, P.N. Brunkov, A.A. Rudenko, N. I. Busleev, A.L. Shakhmin, A.V. Semencha, R.A. Khmelnitsky, N.N. Melnik, I. N. Saraeva, A.A. Nastulyavichus, A.A. Ionin, E.R. Tolordava, Y.M. Romanova, Large-scale laser fabrication of antifouling silicon-surface nanosheet arrays via nanoplasmonic ablative self-organization in liquid CS_2 tracked by a sulfur dopant, ACS Appl. Nano Mater. 1 (2018) 2461–2468, https://doi.org/10.1021/acsanm.8b00392.
[5] A.A. Ionin, S.I. Kudryashov, A.A. Rudenko, L.V. Seleznev, D.V. Sinitsyn, S. V. Makarov, Nonlinear optical feedback for nano- and micropatterning of silicon surface under femtosecond laser irradiation, Opt. Mater. Express 7 (2017) 2793–2807, https://doi.org/10.1364/OME.7.002793.
[6] A. Kiani, K. Venkatakrishnan, B. Tan, Micro/nano scale amorphization of silicon by femtosecond laser irradiation, Opt. Express 17 (2009) 16518–16526, https://doi.org/10.1364/OE.17.016518.
[7] Q. Tan, F. Lu, C. Xue, W. Zhang, L. Lin, J. Xiong, Nano-fabrication methods and novel applications of black silicon, Sens. Actuators, A (2019), https://doi.org/10.1016/j.sna.2019.04.044.
[8] S.K. Sundaram, E. Mazur, Inducing and probing non-thermal transitions in semiconductors using femtosecond laser pulses, Nat. Mater. 1 (2002) 217–224, https://doi.org/10.1038/nmat767.
[9] J. Cao, M. Lancry, F. Brisset, L. Mazerolles, R. Saint-Martin, B. Poumellec, Femtosecond laser-induced crystallization in glasses: growth dynamics for orientable nanostructure and nanocrystallization, Cryst. Growth Des. 19 (2019) 2189–2205, https://doi.org/10.1021/acs.cgd.8b01802.
[10] A.Y. Vorobyev, C. Guo, Direct femtosecond laser surface nano/microstructuring and its applications, Laser Photon. Rev. 7 (2013) 385–407, https://doi.org/10.1002/lpor.201200017.
[11] M. Shen, J.E. Carey, C.H. Crouch, M. Kandyla, H.A. Stone, E. Mazur, High-density regular arrays of nanometer-scale rods formed on silicon surfaces via femtosecond laser irradiation in water, Nano Lett. 8 (2008) 2087–2091, https://doi.org/10.1021/nl080291q.
[12] S.I. Kudryashov, L.V. Seleznev, A.A. Rudenko, A.A. Ionin, In situ supercontinuum nanopatterning of silicon surface by femtosecond laser superfilaments, JETP Letters 109 (2019) 157–162, https://doi.org/10.1134/S0021364019030032.
[13] C.H. Crouch, J.E. Carey, J.M. Warrender, M.J. Aziz, E. Mazur, F.Y. Génin, Comparison of structure and properties of femtosecond and nanosecond laser-structured silicon, Appl. Phys. Lett. 84 (2004) 1850–1852, https://doi.org/10.1063/1.1667004.
[14] R. Buividas, M. Mikutis, S. Juodkazis, Surface and bulk structuring of materials by ripples with long and short laser pulses: recent advances, Prog. Quant. Electron. 38 (2014) 119–156, https://doi.org/10.1016/j.pquantelec.2014.03.002.
[15] M.T. Winkler, M.J. Sher, Y.T. Lin, M.J. Smith, H.F. Zhang, S. Gradecak, E. Mazur, Studying femtosecond-laser hyperdoping by controlling surface morphology, J. Appl. Phys. 111 (2012) 7, https://doi.org/10.1063/1.4709752.
[16] C. Wu, C.H. Crouch, L. Zhao, J.E. Carey, R. Younkin, J.A. Levinson, E. Mazur, R. M. Farrell, P. Gothoskar, A. Karger, Near-unity below-band-gap absorption by microstructured silicon, Appl. Phys. Lett. 78 (2001) 1850–1852, https://doi.org/10.1063/1.1358846.
[17] B.R. Tull, J.E. Carey, E. Mazur, J.P. McDonald, S.M. Yalisove, Silicon surface morphologies after femtosecond laser irradiation, MRS Bull. 31 (2006) 626–633, https://doi.org/10.1557/mrs2006.160.
[18] J. JJ Nivas, E. Allahyari, F. Gesuele, P. Maddalena, R. Fittipaldi, A. Vecchione, R. Bruzzese, S. Amoruso, Influence of ambient pressure on surface structures generated by ultrashort laser pulse irradiation, Appl. Phys. A 124 (2018) 198, https://doi.org/10.1007/s00339-018-1621-6.
[19] I.N. Saraeva, S.I. Kudryashov, V.N. Lednev, S.V. Makarov, S.M. Pershin, A. A. Rudenko, D.A. Zayarny, A.A. Ionin, Single-and multishot femtosecond laser ablation of silicon and silver in air and liquid environments: plume dynamics and surface modification, Appl. Surf. Sci. 476 (2019) 576–586, https://doi.org/10.1016/j.apsusc.2019.01.092.
[20] L.S. Jiao, E.Y.K. Ng, L.M. Wee, H.Y. Zheng, Role of volatile liquids in debris and hole taper angle reduction during femtosecond laser drilling of silicon, Appl. Phys. A 104 (2011) 1081–1084, https://doi.org/10.1007/s00339-011-6374-4.
[21] F. Bai, H.-J. Li, Y.-Y. Huang, W.-Z. Fan, H.-H. Pan, Z. Wang, C.-W. Wang, J. Qian, Y.-B. Li, Q.-Z. Zhao, Polarization effects in femtosecond laser induced amorphization of monocrystalline silicon, Chem. Phys. Lett. 662 (2016) 102–106, https://doi.org/10.1016/j.cplett.2016.08.080.
[22] A.A. Ionin, S.I. Kudryashov, A.O. Levchenko, L.V. Nguyen, I.N. Saraeva, A. A. Rudenko, E.I. Ageev, D.V. Potorochin, V.P. Veiko, E.V. Borisov, D.V. Pankin, D. A. Kirilenko, P.N. Brunkov, Correlated topographic and structural modification on Si surface during multi-shot femtosecond laser exposures: Si nanopolymorphs as potential local structural nanomarkers, Appl. Surf. Sci. 416 (2017) 988–995, https://doi.org/10.1016/j.apsusc.2017.04.215.
[23] F. Costache, S. Kouteva-Arguirova, J. Reif, Sub-damage-threshold femtosecond laser ablation from crystalline Si: surface nanostructures and phase transformation, Appl. Phys. A 79 (2004) 1429–1432, https://doi.org/10.1007/s00339-004-2803-y.
[24] P. Novák, J. Očenášek, L. Prušáková, V. Vavruňková, J. Savková, J. Rezek, Influence of heat generated by a Raman excitation laser on the structural analysis of thin amorphous silicon film, Appl. Surf. Sci. 364 (2016) 302–307, https://doi.org/10.1016/j.apsusc.2015.12.091.
[25] S.V. Gaisler, O.I. Semenova, R.G. Sharafutdinov, B.A. Kolesov, Analysis of Raman spectra of amorphous-nanocrystalline silicon films, Phys. Solid State 46 (2004) 1528–1532, https://doi.org/10.1134/1.1788789.
[26] J.F. Young, J.S. Preston, H.M. van Driel, J.E. Sipe, Laser-induced periodic surface structure. II. Experiments on Ge, Si, Al, and brass, Phys. Rev. B 27 (1983) 1155–1172, https://doi.org/10.1103/PhysRevB.27.1155.
[27] V.K. Malinovsky, V.N. Novikov, N.V. Surovtsev, A.P. Shebanin, Investigation of amorphous states of SiO_2 by Raman scattering spectroscopy, Phys. Solid State 42 (2000) 65–71, https://doi.org/10.1134/1.1131169.
[28] P. Yogi, M. Tanwar, S.K. Saxena, S. Mishra, D.K. Pathak, A. Chaudhary, P. R. Sagdeo, R. Kumar, Quantifying the short-range order in amorphous silicon by Raman scattering, Anal. Chem. 90 (2018) 8123–8129, https://doi.org/10.1021/acs.analchem.8b01352.
[29] R. Le Harzic, D. Dörr, D. Sauer, M. Neumeier, M. Epple, H. Zimmermann, F. Stracke, Large-area, uniform, high-spatial-frequency ripples generated on silicon using a nanojoule-femtosecond laser at high repetition rate, Opt. Lett. 36 (2011) 229–231, https://doi.org/10.1364/OL.36.000229.
[30] A. Ben-Yakar, R.L. Byer, A. Harkin, J. Ashmore, H.A. Stone, M. Shen, E. Mazur, Morphology of femtosecond-laser-ablated borosilicate glass surfaces, Appl. Phys. Lett. 83 (2003) 3030–3032, https://doi.org/10.1063/1.1619560.
[31] J. Jia, M. Li, C.V. Thompson, Amorphization of silicon by femtosecond laser pulses, Appl. Phys. Lett. 84 (2004) 3205–3207, https://doi.org/10.1063/1.1719280.
[32] Y. Izawa, S. Tokita, M. Fujita, M. Nakai, T. Norimatsu, Y. Izawa, Ultrathin amorphization of single-crystal silicon by ultraviolet femtosecond laser pulse irradiation, J. Appl. Phys. 105 (2009), 064909, https://doi.org/10.1063/1.3087754.
[33] T. Mueller, S. Schwertheim, W.R. Fahrner, Crystalline silicon surface passivation by high-frequency plasma-enhanced chemical-vapor-deposited nanocomposite silicon suboxides for solar cell applications, J. Appl. Phys. 107 (2010), 014504, https://doi.org/10.1063/1.3264626.
[34] D. Di Francesca, A. Boukenter, S. Agnello, A. Alessi, S. Girard, M. Cannas, Y. Ouerdane, Resonance Raman of oxygen dangling bonds in amorphous silicon

dioxide, J. Raman Spectrosc. 48 (2017) 230–234, https://doi.org/10.1002/jrs.5006.

[35] K. Kitahara, W. Yeh, A. Hara, Analysis of defects in low-temperature polycrystalline silicon thin films related to surface-enhanced Raman scattering, Jpn. J. Appl. Phys. 57 (2017), 011401, https://doi.org/10.7567/jjap.57.011401.

[36] Z. Sun, M.C. Gupta, A study of laser-induced surface defects in silicon and impact on electrical properties, J. Appl. Phys. 124 (2018) 223103, https://doi.org/10.1063/1.5058143.